Smart Structures and Systems, *Vol. 16, No. 4 (2015) 641-665*
DOI: http://dx.doi.org/10.12989/sss.2015.16.4.641

A simple and efficient 1-D macroscopic model for shape memory alloys considering ferro-elasticity effect

A.R. Damanpack*[1,2], M. Bodaghi[1,2], W.H. Liao[1], M.M. Aghdam[2] and M. Shakeri[2]

[1]*Smart Materials and Structures Laboratory, Department of Mechanical and Automation Engineering, The Chinese University of Hong Kong, Hong Kong, China*
[2]*Thermo-elasticity Center of Excellence, Department of Mechanical Engineering, Amirkabir University of Technology, Tehran, Iran*

(Received July 18, 2014, Revised January 11, 2015, Accepted February 10, 2015)

Abstract. In this paper, a simple and efficient phenomenological macroscopic one-dimensional model is proposed which is able to simulate main features of shape memory alloys (SMAs) particularly ferro-elasticity effect. The constitutive model is developed within the framework of thermodynamics of irreversible processes to simulate the one-dimensional behavior of SMAs under uniaxial simple tension-compression as well as pure torsion+/- loadings. Various functions including linear, cosine and exponential functions are introduced in a unified framework for the martensite transformation kinetics and an analytical description of constitutive equations is presented. The presented model can be used to reproduce primary aspects of SMAs including transformation/orientation of martensite phase, shape memory effect, pseudo-elasticity and in particular ferro-elasticity. Experimental results available in the open literature for uniaxial tension, torsion and bending tests are simulated to validate the present SMA model in capturing the main mechanical characteristics. Due to simplicity and accuracy, it is expected the present SMA model will be instrumental toward an accurate analysis of SMA components in various engineering structures particularly when the ferro-elasticity is obvious.

Keywords: shape memory alloys; constitutive modeling; martensitic transformation; pseudo-elasticity; ferro-elasticity

1. Introduction

Shape memory alloys (SMAs), as one of the most prominent functional metallic materials, are widely used in engineering applications due to their unique thermo-mechanical properties. SMAs present important recoverable inelastic deformation, as a result of the so-called martensitic phase transformation between a high symmetry, parent phase (austenite, A) and a low symmetry, product phase (martensite, M) (Lagoudas 2008). The austenite phase is stable at high temperatures and low stresses, while the martensite phase is stable at low temperatures and/or high stresses. From a macroscopic point of view, the martensite phase exists in two states: self-accommodated or twinned martensite (M^t) and oriented or detwinned martensite (M^d). The twinned martensite is formed by simple cooling under no external loading constraints. The martensite formed in such a

*Corresponding author, Dr., E-mail: ardamanpack@aut.ac.ir

http://www.techno-press.org/?journal=sss&subpage=8 ISSN: 1738-1584 (Print), 1738-1991 (Online)

manner assumes a self-accommodated structure in which the combination of different orientation variants produces no significant macroscopic strain. In contrast, the oriented martensite is produced by an applied load and, consequently, the martensitic variants are preferentially oriented by the direction of the external force. This oriented martensite causes a macroscopic shape change and can be formed either from the phase transformation of austenite under the mechanical loading or from the orientation of twinned martensite.

The thermo-mechanical phase transformation produces two unique effects: shape memory effect (SME) and pseudo-elasticity (PE) (Lagoudas 2008). These phenomena in terms of uniaxial stress-strain response together with their thermo-mechanical loading paths are depicted in Fig. 1. In the absence of stress, the phase transformation is triggered at temperatures addressed by M_s^0, M_f^0, A_s^0 and A_f^0, which represent, respectively, martensite start, martensite finish, austenite start and austenite finish temperatures, see Fig. 1(a). For most alloys, these temperatures can be sorted as $M_f^0 < M_s^0 < A_s^0 < A_f^0$. Fig. 1(b) illustrates the shape memory effect for an SMA material starting as austenite at a temperature $T < A_s^0$. During the loading process, the applied stress induces the formation of detwinned martensite and an inelastic transformation strain. After unloading, the newly formed martensite remains stable, as does the transformation strain. Upon heating the material to temperatures above A_f^0, the material becomes again completely austenitic and the inelastic strain can be fully recovered. Moreover, cooling back to a temperature below M_f^0 can lead to the formation of twinned martensite with no associated shape change observed. A similar stress-strain response as depicted in Fig. 1(b) can also be achieved by starting from twinned martensite, however, it is noted that the detwinning of the twinned martensite $M^t \rightarrow M^d$ does not involve phase transformation and is, in fact, an inelastic deformation process of orientation of martensitic variants. At a temperature $T > A_f^0$, an SMA material behaves pseudo-elastically (Fig. 1(c)). Applying the stress induces the transformation of austenite into detwinned martensite, resulting in an inelastic transformation strain. As the stress is reduced, after an initial elastic response the martensite formed during the loading process transforms back to the austenite, the inelastic strain is accordingly recovered, and the stress-strain diagram exhibits the characteristic hysteretic loop as shown in Fig. 1(c).

Experimental observations of SMAs undergoing cyclic loading via thermal activation under constant stress or operating in the pseudo-elastic regime have shown that a significant part of the developed strain is not recovered on unloading and accumulates with every transformation cycle (Lagoudas 2008, Saleeb *et al.* 2013). This effect is well-known as transformation-induced plasticity and is attributed to the development of irrecoverable plastic strains during the thermo-mechanical cycling of SMAs undergoing phase transformation until saturation takes place.

In addition to the main features of SMAs including the martensite phase transformation/orientation, transformation-induced plasticity, pseudo-elastic response and shape memory effect, these materials reproduce the so-called ferro-elasticity (FE). A schematic stress-strain response of the FE effect of SMAs for $T < A_s^0$ is shown in Fig. 2. The ferro-elasticity effect allows recovery of an inelastic residual strain obtained from the first tensile loading-unloading stage at temperatures below A_f^0 by application of a stress with opposite sign (i.e., compressive stress). The ferro-elasticity feature of SMAs is associated with the stress-induced phase transformation between detwinned martensite and twinned

martensite/austenite for $T < A_f^0$. In fact, the previously developed detwinned martensite by tensile stress is first transformed to twinned martensite/austenite when the compressive stress is applied (Panico and Brinson 2007). As the compressive load further increases, the twinned martensite/austenite is then transformed to detwinned martensite.

The unique aspects of SMAs including shape memory effect, ferro-elasticity, pseudo-elasticity, large recovery strain and stress, high damping capacity and adaptive properties make them attractive candidates for use in intelligent/smart engineering structures (Lagoudas 2008, Seelecke and Muller 2004). SMAs can be easily fabricated into various forms such as fibers, wires, ribbons and thin films. In the most common applications, SMAs are used as a single material, externally attached or surface-mounted/embedded in a soft/stiff matrix, while electrical current is normally employed to induce the thermally driven transformation. The shape memory hybrid composites, with either surface-bonded or embedded SMA components, have proved to be unique material systems that provide tremendous potential for creating new paradigms for material-structural interactions (Lagoudas 2008, Seelecke and Muller 2004). For instance, the metallic and concrete matrix shape memory composites have demonstrated varying success in many fields including shape and position control (Daghia *et al.* 2010, Roh *et al.* 2004) and active vibration control (Shahria Alam *et al*. 2009, Youssef and Elfeki 2012, Zhang and Zhao 2007).

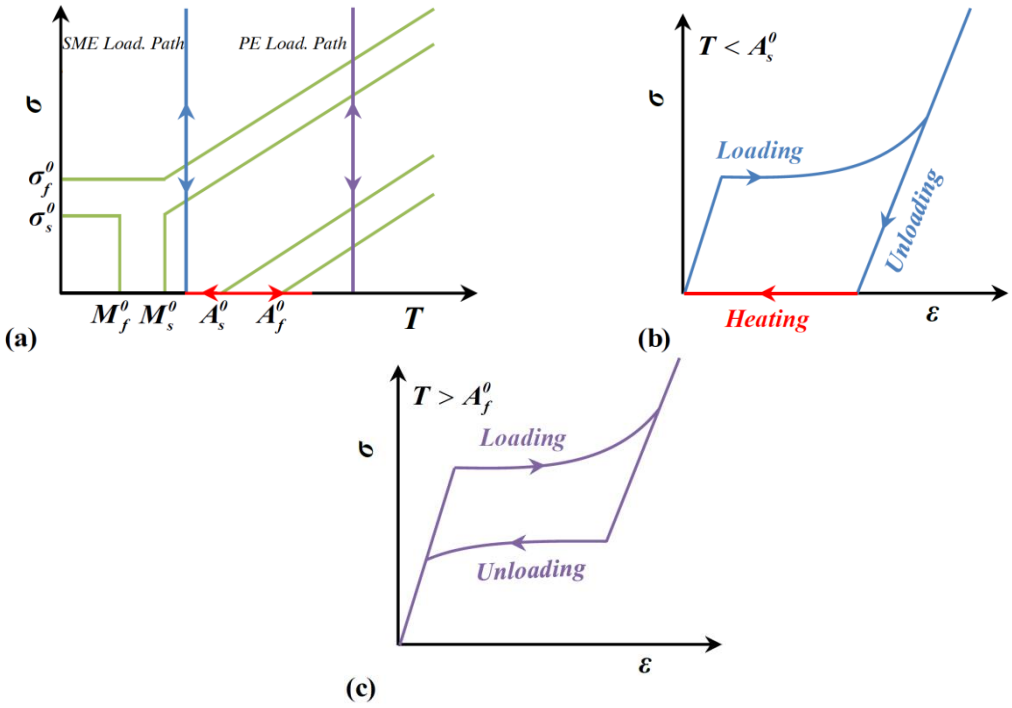

Fig. 1 (a) Schematic of a stress-temperature phase diagram and shape memory effect and pseudo-elastic loading paths, (b) stress-strain diagram representing SME, (c) stress-strain curve of PE response

Note that polymeric matrix is difficult to apply for the slip effects due to strain differences between dilatation of polymer and SMA transformation. SMAs could also be good candidates for solid-state dampers for the oscillation mitigation of bridge stay cables and civil structures because of their large recoverable strain, hysteresis and reasonable fatigue-life (BenMekki and Auricchio 2011, Casciati and Hamdaoui 2008, Carreras *et al*. 2011, Torra *et al*. 2013).

In order to simulate and predict the main features of SMAs, numerous research studies have been dedicated to develop an efficient and robust mathematical model of SMAs. The proposed models can be generally classified into three major categories including: microscopic thermodynamics, micromechanics based macroscopic and phenomenological macroscopic models according to the scale at which the SMA mechanical behavior is described. Phenomenological macroscopic models (macro models) only use macroscopic quantities to describe the state of the system and they are usually based on phenomenological thermodynamics and curve fitting of the experimental data, see for example (Brinson 1993, Boyd and Lagoudas 1996, Bekker and Brinson 1998, Bodaghi *et al.* 2013, Chung *et al.* 2007, Liang and Rogers 1990, Lagoudas *et al.* 1996, Panico and Brinson 2007, Tanaka 1986) among others. Macro models are generally more suitable for engineering applications due to their simplicity and computational efficiency, but they can only describe the global mechanical response while all microscopic details are disregarded (Lagoudas 2008).

In recent years, the macro constitutive modeling of SMAs has been an active research subject. Some research works were directed to develop three/two-dimensional (3/2-D) phenomenological macroscopic models in capturing the main effects of SMAs (Boyd and Lagoudas 1996, Bodaghi *et al.* 2013, Lagoudas *et al.* 1996, Panico and Brinson 2007). For instance, Boyd and Lagoudas (1996) used the volume fraction of martensite as internal variable and a transformation evolution equation to connect it with the transformation strain. They introduced a polynomial hardening function to express the transformation kinetics. Bodaghi *et al.* (2013) proposed a phenomenological model which accounts for the effect of biaxial stress states and non-proportional loading histories. The proposed model was able to simulate the reorientation of previously developed oriented martensite when the load direction changed through biaxial non-proportional loadings. It should be noted that 3/2-D models are not widely used in engineering applications, because the developed models are too complicated and require definition of many parameters. Although these models can be simplified to be used for one-dimensional (1-D) applications such as SMA fibers, wires, ribbons and thin films, it is not reasonable to use 3/2-D models for 1-D applications.

In contrast to 3/2-D models, 1-D models (Brinson 1993, Bekker and Brinson 1998, Chung *et al.* 2007, Liang and Rogers 1990, Tanaka 1986) have also been developed to properly capture main aspects of SMAs. One advantage of these models is that parameters are engineering-based and simply determined by typical thermo-mechanical experiments. One of the first 1-D models for SMAs under uniaxial tension or compression loads was presented by Tanaka (1986). Stress, strain, temperature and martensite volume fraction were used as state variables. Also, phase transformation kinetics was expressed with an exponential function for the evolution equation of the martensite volume fraction during the phase transformation. Liang and Rogers (1990) formulated Tanaka model by using a cosine function to describe the transformation kinetics instead of the exponential function. Lagoudas *et al*. (1996) provided a unified framework for the models of Boyd and Lagoudas (1996), Liang and Rogers (1990) and Tanaka (1986). A major drawback of the models proposed in (Boyd and Lagoudas 1996, Liang and Rogers 1990, Lagoudas *et al*. 1996, Tanaka 1986) is that these models describe only the phase transformation from detwinned martensite to austenite and vice versa. These models were not able to reproduce the orientation

(detwinning) of twinned martensite that is responsible for the shape memory effect at low temperatures. Brinson (1993) extended Liang and Rogers model to include the effect of the martensite orientation by separating the martensite fraction into two parts: stress-induced martensite (detwinned martensite) and temperature-induced martensite (twinned martensite). Brinson model used cosine functions for the martensite transformation kinetics. These functions, under certain conditions, lead to an inadmissible martensite fraction when the temperature decreases at low temperature $(T < M_s^0)$. After Brinson original model, Bekker and Brinson (1998) developed a consistent mathematical description of the martensite fraction evolution during athermal thermo-elastic phase transformation in an SMA induced by a general thermo-mechanical loading. Though the Bekker and Brinson kinetics is robust and does not permit the volume fractions to exceed unity, due to simplicity in Brinson original model, Chung *et al*. (2007) suggested simple modified transformation kinetics for this model and verified the proposed formulae numerically.

Among 1-D models, the phenomenological models proposed by Tanaka (1986), Liang and Rogers (1990) and Brinson (1993) were the most popular models. Due to their simplicity, many researchers employed these models to predict the response of SMAs in structural engineering applications (Roh *et al*. 2004, Zhang and Zhao 2007). It should be mentioned that these models are not able to simulate the ferro-elasticity effect when the pre-strained SMAs undergo a compressive stress at temperatures below A_f^0, see Fig. 2. It is obvious that the stress in SMA devices can be varied from tension to compression and vice versa during thermo-mechanical loadings. Therefore, introducing a simple 1-D SMA model capable of simulating the ferro-elasticity effect seems to be helpful for use in engineering applications, especially in shape memory hybrid composites.

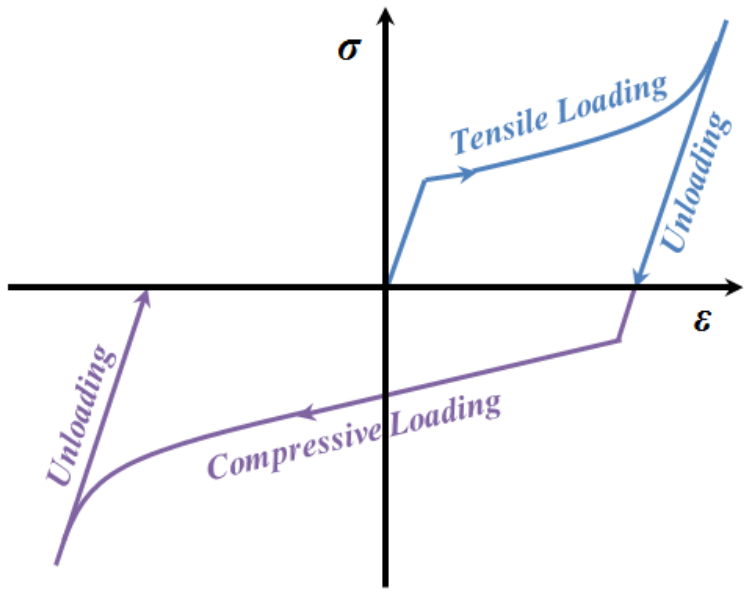

Fig. 2 Schematic of stress-strain response of ferro-elasticity feature of SMAs for $T < A_s^0$

In the present research, a simple and efficient 1-D phenomenological macroscopic model of SMAs is proposed to simulate main features of SMAs including the martensite phase transformation/orientation, shape memory effect, pseudo-elasticity and in particular ferro-elasticity. The SMA constitutive model is developed within the framework of continuum thermodynamics of irreversible processes and a straightforward algorithm is addressed to formulate the 1-D behavior of SMAs under uniaxial simple tension-compression, pure torsion+/- and also thermal loadings. Linear, cosine and exponential functions are nominated in a unified framework to interpolate martensite transformation kinetics and an analytical description of the constitutive equations is presented. An easy procedure for specifying the kinetic and material parameters of the model is introduced in detail. The model is first validated by comparing the predicted results with experimental data reported in the open literature for uniaxial tension and torsion tests of SMA materials. Then, a finite element formulation is developed to simulate experimental bending tests of thin SMA beams under transverse loadings. Finally, the proposed model and finite element solution are employed to study the bending response of SMA beams under various thermo-mechanical loadings.

2. Theoretical formulations

In this section, a simple and efficient 1-D SMA constitutive model is developed within the theory of irreversible thermodynamics in the realm of small strain regime. A straightforward algorithm is introduced to develop analytical relationships for the 1-D thermo-mechanical behavior of SMAs under uniaxial tension-compression, pure torsion+/- and thermal loadings.

2.1 Assumptions

The total martensite fraction, ξ, can be expressed as the sum of stress-induced and temperature-induced parts

$$\xi = \xi_S + \xi_T, \qquad 0 \le \xi_S \le 1, \;\; 0 \le \xi_T \le 1, \;\; 0 \le \xi \le 1 \tag{1}$$

where ξ_T represents the fraction of the material that is purely temperature-induced martensite with multiple variants, and ξ_S denotes the fraction of the material that has been transformed by the stress into a single martensitic variant.

Assuming small strains, an additive decomposition of the total strain tensor into elastic and transformation parts is adapted as:

$$\boldsymbol{\varepsilon} = \boldsymbol{\varepsilon}_e + \boldsymbol{\varepsilon}_{tr} \tag{2}$$

where $\boldsymbol{\varepsilon}_e$ denotes the elastic contribution to the total strain of SMA and $\boldsymbol{\varepsilon}_{tr}$ plays the role of describing the strain associated to the phase transformation between austenite/twinned martensite and detwinned martensite.

The transformation and detwinning of martensite variants occur mainly through a shear lattice distortion (Lagoudas 2008). Therefore, it is assumed that the transformation strain tensor $\boldsymbol{\varepsilon}_{tr}$ is traceless and is a measure of strain associated to the phase transformation. When $\|\boldsymbol{\varepsilon}_{tr}\| = 0$, it can

be said that the material is in its parent phase, i.e., austenite or twinned martensite, whereas $\|\boldsymbol{\varepsilon}_{tr}\| = \beta$ shows that the material is in its product phase, i.e., detwinned martensite, and when $0 \le \|\boldsymbol{\varepsilon}_{tr}\| \le \beta$, a mixture of both parent and product phases can be observed in the material. Since β is the amount of the strain associated with the detwinned martensitic variant, $\boldsymbol{\varepsilon}_{tr}$ is related to the volumetric fraction ξ_S as

$$\|\boldsymbol{\varepsilon}_{tr}\| = \xi_S \beta \tag{3}$$

where $\|\ \|$ is the usual Euclidean norm. Eq. (3) shows that the transformation strain can also be interpreted as the mean strain of the mixture of austenite (or twinned martensite) and detwinned martensite phases.

In the case of uniaxial tension and torsion loadings, the transformation strain tensor $\boldsymbol{\varepsilon}_{tr}$ which is traceless can be expressed as

$$\text{Tension}: \ \boldsymbol{\varepsilon}_{tr} = \begin{bmatrix} \varepsilon_{tr} & 0 & 0 \\ 0 & -\frac{1}{2}\varepsilon_{tr} & 0 \\ 0 & 0 & -\frac{1}{2}\varepsilon_{tr} \end{bmatrix} \tag{4a}$$

$$\text{Torsion}: \ \boldsymbol{\varepsilon}_{tr} = \begin{bmatrix} 0 & 0 & 0 \\ 0 & 0 & \frac{1}{2}\gamma_{tr} \\ 0 & \frac{1}{2}\gamma_{tr} & 0 \end{bmatrix} \tag{4b}$$

where ε_{tr} and γ_{tr} are transformation normal and shear strains, respectively.

As mentioned before, the detwinning process results in a residual strain. If ε_L is corresponded to the maximum transformation strain reached at the end of transformation during a uniaxial tension test, with aid of Eqs. (3) and (4(a)), the following relation for the parameter β can be obtained

$$\beta = \sqrt{3/2}\varepsilon_L \tag{5}$$

Finally, by substituting (5) into (3) the detwinned martensite fraction can be expressed as

$$\xi_S = \frac{\|\boldsymbol{\varepsilon}_{tr}\|}{\sqrt{3/2}\varepsilon_L} \tag{6}$$

2.2 Model description

The main purpose of the present study is to develop 1-D SMA model for uniaxial tension-compression and torsion+/- loadings. The detwinned martensite fraction for these two cases can be obtained from (6) as

$$\xi_S = \frac{|\varepsilon_{tr}|}{\varepsilon_L} \tag{7a}$$

$$\xi_S = \frac{|\gamma_{tr}|}{\sqrt{3}\varepsilon_L} \tag{7b}$$

Eq. (7) reveals that the stress-induced martensite fraction ξ_S has a similar form for uniaxial cases. In the following, the 1-D SMA model will be developed for the case of the uniaxial simple tension-compression loading. It is obvious that the formulation is valid for the uniaxial pure torsion case only by replacing $\varepsilon_{tr}, \varepsilon_e, \sigma, E$ by $\gamma_{tr}/\sqrt{3}, \gamma_e/\sqrt{3}, \sqrt{3}\tau, 3G$, respectively ($E$ and G are extension and shear moduli, and σ and τ denote normal and shear stresses).

The rate of the detwinned martensite fraction can be written from (7a) as

$$\dot{\xi}_S = \dot{\varepsilon}_{tr}\,\mathrm{sgn}(\varepsilon_{tr})/\varepsilon_L \tag{8}$$

where the signum function is defined as

$$\mathrm{sgn}(x) = \begin{cases} 1 & if\ x > 0 \\ 0 & if\ x = 0 \\ -1 & if\ x < 0 \end{cases} \tag{9}$$

The model assumes the elastic strain ε_e and the absolute temperature, T, as control variables and the volume fraction of twinned martensite ξ_T and the volume fraction of detwinned martensite ξ_S as internal variables. In order to establish the Helmoltz free energy of a polycrystalline SMA material, ψ, a mechanistic decomposition to three dominating contributions, elastic energy ψ^e, chemical energy ψ^{chem} and configurational energy ψ^{config}, is used as

$$\psi = \psi^e + \psi^{chem} + \psi^{config} \tag{10}$$

To derive the elastic energy contribution, the polycrystalline material is assumed to be elastically isotropic with a homogeneous distribution of stress in austenite and martensite. Neglecting thermal expansion, the elastic energy term can be expressed as

$$\psi^e = \frac{1}{2\rho} E \varepsilon_e^2 \tag{11}$$

where ρ and E denote the material density and the isotropic elasticity modulus, which are assumed to be the same for all phases.

Following the general scheme summarized by Patoor *et al*. (2006), the rule of mixtures is used to determine the free energy contribution ψ^{chem} as

$$\psi^{chem} = (1-\xi)\psi^A + \xi\psi^M \tag{12}$$

where ψ^A and ψ^M are specific free energies of austenite and martensite phases at stress-free

conditions, respectively. ψ^M is considered to be the same for both detwinned and twinned martensite. Adopting a standard form (e.g., Lexcellent *et al*. 2006, Panico and Brinson 2007), the specific free energies can be written as

$$\psi^i = u_0^i - Ts_0^i + c^i\left[T - T_0 - T\ln(T/T_0)\right] \ , \ \ i = A,M \tag{13}$$

where $c^i\,(i = A,M)$ indicates the specific heat at constant volume for austenite and martensite phases. Also, u_0^i and $s_0^i\,(i = A,M)$ denote the specific internal energy and entropy of the corresponding phase at the equilibrium temperature T_0. It is a critical temperature at which the free energies of austenite and martensite phases are equal i.e., $\psi^A(T_0) = \psi^M(T_0)$ (Sedlák *et al*. 2012). This results in $T_0 = \Delta u_0 / \Delta s_0$ where $\Delta u_0 = u_0^A - u_0^M$ and $\Delta s_0 = s_0^A - s_0^M$. By substituting (13) into (12), the chemical energy can be rewritten as

$$\psi^{chem} = u_0^A - Ts_0^A + c^A\left[T - T_0 - T\ln(T/T_0)\right] + \xi\Delta s_0(T - T_0) - \xi\Delta c\left[T - T_0 - T\ln(T/T_0)\right] \tag{14}$$

where $\Delta c = c^A - c^M$. It is known that $\Delta c << \Delta s_0$ (Sedlák *et al*. 2012). Due to this fact, the last term of (14) can be neglected.

The configurational energy representing interactions that appear between the phases typically the incompatibilities between deformations, is assumed to depend only on ξ_S according to the following quadratic form

$$\psi^{config} = \frac{1}{2}H_S\xi_S^2 \tag{15}$$

where H_S is a material parameter which controls the initial hardening during phase transformation.

Finally, by substituting relations (11), (14) and (15) into (10), the Helmoltz free energy of the three phase system can be written as

$$\begin{aligned}\psi(\varepsilon_e, T, \xi_S, \xi_T) = {} & \frac{1}{2\rho}E\varepsilon_e^2 + u_0^A - Ts_0^A + \xi_T\Delta s_0(T - T_0) \\ & + \xi_S\Delta s_0\left\langle T - T_0\right\rangle + c^A\left[T - T_0 - T\ln(T/T_0)\right] + \frac{1}{2}H_S\xi_S^2\end{aligned} \tag{16}$$

It should be noted that in the energy contribution deriving from ξ_S, the positive part function $\langle\bullet\rangle$ is introduced and defined as $\langle x\rangle = (x + |x|)/2$. This assumption allows the critical stress for nucleation of detwinned martensite to plateau at lower temperatures, as experimentally observed (Lagoudas 2008).

According to the second law of thermodynamics, the mechanical dissipation inequality by considering the positiveness of the thermal dissipation is obtained as

$$\rho D_{mech} = \sigma\dot{\varepsilon} - \rho\dot{\psi} - \rho s\dot{T} \geq 0 \tag{17}$$

where s denotes the specific entropy. Also, the superposed dot indicates the derivative of a

quantity with respect to time.

Introducing Eq. (2) into the inequality (17) together with the definition of free energy in (16), the mechanical dissipation inequality can be rewritten as

$$\rho D_{mech} = -\rho\left(s + \frac{\partial \psi}{\partial T} \right)\dot{T} + \left(\sigma - \rho \frac{\partial \psi}{\partial \varepsilon_e} \right)\dot{\varepsilon}_e + \left(\sigma \varepsilon_L \operatorname{sgn}(\varepsilon_{tr}) - \rho \frac{\partial \psi}{\partial \xi_S} \right)\dot{\xi}_S - \rho \frac{\partial \psi}{\partial \xi_T}\dot{\xi}_T \geq 0 \tag{18}$$

This inequality must be satisfied for any $\dot{T}$ and $\dot{\varepsilon}_e$ which yields to the following state equations

$$\begin{aligned} \sigma &= \rho \frac{\partial \psi}{\partial \varepsilon_e} = E\varepsilon_e \\ s &= -\frac{\partial \psi}{\partial T} = s_0^A - \Delta s_0 (\xi_T + \xi_S \frac{\langle T - T_0 \rangle}{|T - T_0|}) + c^A \ln(T / T_0) \end{aligned} \tag{19}$$

On the basis of the definition of free energy in (16), the dissipation inequality (18) can be now expressed as

$$\rho D_{mech} / \varepsilon_L = X_S \dot{\xi}_S + X_T \dot{\xi}_T \geq 0 \tag{20}$$

where the thermo-dynamical dissipative forces X_S and X_T are defined as

$$\begin{aligned} X_S &= \sigma \operatorname{sgn}(\varepsilon_{tr}) - \frac{\rho \Delta s_0}{\varepsilon_L} \langle T - T_0 \rangle - \frac{\rho H_S}{\varepsilon_L} \xi_S \\ X_T &= -\frac{\rho \Delta s_0}{\varepsilon_L} (T - T_0) \end{aligned} \tag{21}$$

For the internal variables ξ_S and ξ_T, the following limit functions are considered:

$$F_S = X_S \operatorname{sgn}(X_S) - Y_S^{f/r}(\xi_S) \tag{22a}$$

$$F_T = X_T \operatorname{sgn}(X_T) - Y_T^{f/r}(\xi_T, \sigma) \tag{22b}$$

where $Y_S^{f/r}(\xi_S)$ and $Y_T^{f/r}(\xi_T, \sigma)$ are functions that govern the kinetics of forward/reverse phase transformations. The model is finally completed by the classical Kuhn-Tucker and consistency conditions, respectively, as follows

$$\begin{cases} F_S < 0 \ , \ \dot{\xi}_S = 0 \\ \quad or \\ F_S = 0 \ , \ \dot{\xi}_S \neq 0 \end{cases} \qquad \begin{cases} F_T < 0 \ , \ \dot{\xi}_T = 0 \\ \quad or \\ F_T = 0 \ , \ \dot{\xi}_T \neq 0 \end{cases} \tag{23a}$$

$$\begin{cases} \dot{F}_S < 0 \ , \ \dot{\xi}_S = 0 \\ \qquad or \qquad if \quad F_S = 0 \\ \dot{F}_S = 0 \ , \ \dot{\xi}_S \neq 0 \end{cases} \qquad \begin{cases} \dot{F}_T < 0 \ , \ \dot{\xi}_T = 0 \\ \qquad or \qquad if \quad F_T = 0 \\ \dot{F}_T = 0 \ , \ \dot{\xi}_T \neq 0 \end{cases} \tag{23b}$$

Conditions (23) express the physical requirements, elaborated upon above, that the stress state stays on the yield surface as long as martensitic transformation takes place $F_i = 0 (i = S,T)$ (Simo and Hughes 1998).

The kinetics of the stress-induced forward/reverse phase transformation can be expressed in the general form as

$$Y_S^{f/r}(\xi_S) = \begin{cases} Y_{S0}^f N_0^f(\xi_S) + Y_{S1}^f N_1^f(\xi_S) & for \ \dot{\xi}_S > 0 \\ Y_{S0}^r N_0^r(\xi_S) + Y_{S1}^r N_1^r(\xi_S) & for \ \dot{\xi}_S < 0 \end{cases} \tag{24}$$

where $N_0^{f/r}(\xi_S)$ and $N_1^{f/r}(\xi_S)$ refer to interpolation/shape functions. Also $Y_{S0}^{f/r}$ and $Y_{S1}^{f/r}$ are, respectively, the values of $Y_S^{f/r}$ at $\xi_S = 0$ and $\xi_S = 1$, related to the beginning and end of transformation and describe the kinetics of the stress-induced forward/reverse transformation.

Similar to all other interpolants, the shape functions should satisfy the condition

$$N_i^{f/r}(\xi_{Sj}) = \begin{cases} 1 & if \ i = j \\ 0 & if \ i \neq j \end{cases} \quad for i, j = 0,1 \tag{25}$$

where $\xi_{S0} = 0$ and $\xi_{S1} = 1$. In addition, the interpolation functions satisfy the property, known as the partition of unity

$$N_0^{f/r} + N_1^{f/r} = 1 \tag{26}$$

In the present work, a variety of well-known functions including: linear, cosine and exponential functions are introduced to interpolate stress-induced transformation/orientation kinetics $(Y_S^{f/r})$. The interpolation functions for these cases can be expressed as

for the forward transformation:

$$\begin{cases} \text{Linear}: N_0^f(\xi_S) = 1 - \xi_S \ , \ \ N_1^f(\xi_S) = \xi_S \\ \text{Cosine}: N_0^f(\xi_S) = \dfrac{2}{\pi}\cos^{-1}\xi_S, \ \ N_1^f(\xi_S) = 1 - \dfrac{2}{\pi}\cos^{-1}\xi_S \\ \text{Exponential}: N_0^f(\xi_S) = 1 + \dfrac{1}{n}\ln(1-\xi_S) \ , \ \ N_1^f(\xi_S) = -\dfrac{1}{n}\ln(1-\xi_S) \ , n > 0 \end{cases} \tag{27}$$

for the reverse transformation:

$$\begin{cases} \text{Linear}: N_0^r(\xi_S)=1-\xi_S \ , \ \ N_1^r(\xi_S)=\xi_S \\ \text{Cosine}: N_0^r(\xi_S)=1-\dfrac{2}{\pi}\cos^{-1}(1-\xi_S), \ \ N_1^r(\xi_S)=\dfrac{2}{\pi}\cos^{-1}(1-\xi_S) \\ \text{Exponential}: N_0^r(\xi_S)=-\dfrac{1}{n}\ln(\xi_S) \ , \ \ N_1^r(\xi_S)=1+\dfrac{1}{n}\ln(\xi_S) \ , \ n>0 \end{cases} \tag{28}$$

It should be mentioned that the exponential formulae become singular at $\xi_S=0$ and 1. To overcome this defect, the quantities $\xi_S=1-e^{-n}$ and $\xi_S=e^{-n}$ are used for the complete martensitic and austenitic states, respectively. The unknown positive parameter n can be determined according to a digit approximated for zero. For instance, $n=7$ is used in the present study to approximate zero with 0.001 .

In order to describe temperature-induced forward/reverse phase transformation kinetics $(Y_T^{f/r})$, the following linear approximation can be adopted (Panico and Brinson 2007)

$$Y_T^{f/r}(\xi_T,\sigma)=\begin{cases} \dfrac{\rho c^f}{\varepsilon_L}\xi_T & for \quad \dot{\xi}_T>0 \\ \dfrac{Y_{T0}^r}{\varepsilon_L}+|\sigma|+\dfrac{\rho c^r}{\varepsilon_L}(1-\xi_T) & for \quad \dot{\xi}_T<0 \end{cases} \tag{29}$$

where $c^{f/r}$ and Y_{T0}^r are coefficients that describe the kinetics of the forward/reverse transformation.

2.3 Parameter determination

In this section, a simple procedure for identifying the parameters of the model is described in detail.

The material parameters $c^f, c^r, Y_{T0}^r, T_0, \Delta s_0$ and kinetic parameters $Y_{S0}^f, Y_{S1}^f, Y_{S0}^r, Y_{S1}^r, H_S$ are related to the common quantities that characterize a uniaxial phase kinetics diagram. For instance, four characteristic temperatures can be written in terms of c^f, c^r, Y_{T0}^r, T_0 and Δs_0 using conditions

$$\begin{aligned} &F_T^f=0 && @\ \xi_T=0,\ T=M_s^0 \Rightarrow M_s^0=T_0 \\ &F_T^f=0 && @\ \xi_T=1,\ T=M_f^0 \Rightarrow M_f^0=T_0-\frac{c^f}{\Delta s_0} \\ &F_T^r=0 && @\ \xi_T=1,\ T=A_s^0,\ \sigma=0 \Rightarrow A_s^0=T_0+\frac{Y_{T0}^r}{\rho\Delta s_0} \\ &F_T^r=0 && @\ \xi_T=0,\ T=A_f^0,\ \sigma=0 \Rightarrow A_f^0=\frac{(Y_{T0}^r+\rho c^r)}{\rho\Delta s_0}+T_0 \end{aligned} \tag{30}$$

It should be mentioned that, in reality, the forward/reverse phase transformations do not begin exactly at T_0, but, in the absence of stress, at a temperature M_s^0 / A_s^0, which is lower/higher than

T_0 (Patoor *et al*. 2006). As it can be found from (30), the model predicts austenite start temperature above T_0 $(i.e., A_s^0 > T_0)$ which is consistent with the reality. On the other hand, the model predicts that forward phase transformation begins exactly at T_0 $(i.e., M_s^0 = T_0)$ which is in contrast with reality $M_s^0 < T_0$. A similar contradiction was also observed by Panico and Brinson (2007). Since the main focus of the study is to develop a simple and efficient constitutive SMA model, this contradiction is ignored.

Moreover, in the case of an applied stress, σ, one obtains

$$\begin{aligned} A_s &= A_s^0 + \frac{|\sigma|\varepsilon_L}{\rho \Delta s_0} \\ A_f &= A_f^0 + \frac{|\sigma|\varepsilon_L}{\rho \Delta s_0} \end{aligned} \tag{31}$$

From Eq. (31), the conventional slope of the transformation lines to austenite in the uniaxial phase kinetics diagram can be easily obtained as

$$C_A = \rho \Delta s_0 / \varepsilon_L \tag{32}$$

By knowing the parameter Δs_0 through entropic consideration and the mass density ρ and the parameter ε_L, the quantity C_A is determined by Eq. (32). Moreover, Eq. (30) allows determination of the parameters c^f, c^r, Y_{T0}^r and T_0 as a function of the SMA characteristic temperatures and entropy

$$\begin{aligned} c^f &= \Delta s_0 (M_s^0 - M_f^0) \\ c^r &= \Delta s_0 (A_f^0 - A_s^0) \\ Y_{T0}^r &= \rho \Delta s_0 (A_s^0 - M_s^0) \\ T_0 &= M_s^0 \end{aligned} \tag{33}$$

The kinetic parameters $Y_{S0}^f, Y_{S1}^f, Y_{S0}^r$ and Y_{S1}^r can be defined from the following conditions:

$$\begin{cases} F_S^f = 0 & @\ \xi_S = 0, \sigma = \sigma_s^0, T = M_s^0 \Rightarrow Y_{S0}^f = \sigma_s^0 \operatorname{sgn}(\varepsilon_{in}) \\ F_S^f = 0 & @\ \xi_S = 1, \sigma = \sigma_f^0, T = M_s^0 \Rightarrow Y_{S1}^f = \sigma_f^0 \operatorname{sgn}(\varepsilon_{in}) - \tilde{\sigma} \\ F_S^r = 0 & @\ \xi_S = 1, \sigma = 0, T = A_s^0 \Rightarrow Y_{S1}^r = C_A (A_s^0 - M_s^0) + \tilde{\sigma} \\ F_S^r = 0 & @\ \xi_S = 0, \sigma = 0, T = A_f^0 \Rightarrow Y_{S0}^r = C_A (A_f^0 - M_s^0) \end{cases} \tag{34}$$

where σ_s^0 is the minimum stress required for the initiation of martensite orientation at temperatures below M_s^0; and also σ_f^0 is the high stress level which will result in complete orientation of martensite. Also, the parameter $\tilde{\sigma}$ is equal to $\rho H_S / \varepsilon_L$ and can be identified as a relative stress.

In a similar way, it is possible to derive analytical relations for the critical stresses at the beginning and end of the forward/reverse phase transformation as functions of temperature. To this end, Eq. (34) together with the following conditions can be employed which results in

$$\begin{cases} F_S^f = 0 & @\ \xi_S = 0, \sigma = \sigma_s^M \Rightarrow \sigma_s^M = \sigma_s^0 + C_M\ \mathrm{sgn}(\varepsilon_{in})\left\langle T - M_s^0 \right\rangle \\ F_S^f = 0 & @\ \xi_S = 1, \sigma = \sigma_f^M \Rightarrow \sigma_f^M = \sigma_f^0 + C_M\ \mathrm{sgn}(\varepsilon_{in})\left\langle T - M_s^0 \right\rangle \\ F_S^r = 0 & @\ \xi_S = 1, \sigma = \sigma_s^A \Rightarrow \sigma_s^A = C_A\ \mathrm{sgn}(\varepsilon_{in})(T - A_s^0) \\ F_S^r = 0 & @\ \xi_S = 0, \sigma = \sigma_f^A \Rightarrow \sigma_f^A = C_A\ \mathrm{sgn}(\varepsilon_{in})(T - A_f^0) \end{cases} \tag{35}$$

where σ_s^M and σ_f^M denote the stress levels at which the martensite transformation initiates and completes, respectively. Similarly, as the SMA is unloaded, the stress levels at which the material initiates and completes its reverse transformation to austenite are determined by σ_s^A and σ_f^A, respectively. It is worth noting that the present model yields the same line slope for the forward and reverse transformation i.e. $C_A = C_M = \rho \Delta s_0 / \varepsilon_L \cong C$.

By focusing on the presented relations in this section, it can be found that the parameters $c^f, c^r, Y_{T0}^r, T_0, Y_{S0}^f, Y_{S1}^f, Y_{S0}^r$ and Y_{S1}^r defined by Eqs. (33) and (34) can be described as functions of four characteristic temperatures and the quantities $C, \sigma_s^0, \sigma_f^0, \widetilde{\sigma}$ and ε_L. These five material quantities are calibrated to match the uniaxial stress-strain response for simple tension-compression and/or pure torsion+/- experimental tests. Finally, it can be concluded that the present SMA model is operated by a set of 12 model inputs consisting of $M_f^0, M_s^0, A_s^0, A_f^0, C, \sigma_s^0, \sigma_f^0, \widetilde{\sigma}, E, \nu, \rho$ and ε_L.

2.4 Time-discrete frame

In this section, the proposed constitutive model is used to update twinned and detwinned martensite fractions under strain, stress or temperature control conditions. It is interesting to note that the evolution of detwinned martensite from Eq. (22(a)) which is coupled with the transformation strain through Eq. (8) is independent of the evolution of twinned martensite (22b).

Assuming the state $(\varepsilon^n, \xi_S^n, \xi_S^n, \varepsilon_{tr}^n)$ is known at time t^n, the actual total strain ε^{n+1} and temperature T^{n+1} at t^{n+1}, the updated values $(\sigma^{n+1}, \xi_S^{n+1}, \varepsilon_{tr}^{n+1})$ can be computed from the following time-discrete system

$$\begin{aligned} &\sigma^{n+1} = E(\varepsilon^{n+1} - \varepsilon_{tr}^{n+1}) \\ &X_S^{n+1} = \sigma^{n+1}\ \mathrm{sgn}(\varepsilon_{tr}^{n+1}) - C\left\langle T^{n+1} - M_s^0 \right\rangle - \widetilde{\sigma}\xi_S^{n+1} \\ &F_S^{n+1} = X_S^{n+1}\ \mathrm{sgn}(X_S^{n+1}) - Y_S^{f/r}(\xi_S^{n+1}) \\ &\varepsilon_{tr}^{n+1} = \varepsilon_{tr}^n + (\xi_S^{n+1} - \xi_S^n)\ \mathrm{sgn}(\varepsilon_{tr}^{n+1})\varepsilon_L \end{aligned} \tag{36}$$

along with the requirements

$$F_S^{n+1} < or = 0\ ,\ (\xi_S^{n+1} - \xi_S^n) = or \neq 0\ ,\ F_S^{n+1}(\xi_S^{n+1} - \xi_S^n) = 0 \tag{37}$$

It should be mentioned that an implicit backward-Euler scheme is used to integrate the flow rule. The solution of the discrete model is performed by using an elastic-predictor inelastic-corrector return map procedure (Simo and Hughes 1998). In the first step, an elastic trial

stress is computed by assuming that the material behaves elastically during the time step $(\sigma^{trial} = E(\varepsilon^{n+1} - \varepsilon_{tr}^{n}))$. Then, based on this elastic prediction the limit function F_S^{trial} is computed. If the limit function is negative, then the material response is elastic and the trial stress (σ^{trial}) is taken as the updated stress (σ^{n+1}). If the limit function has a positive value, then an inelastic correction for the material response needs to be computed. The solution of governing equation (36) directly depends on the nature of stress-induced transformation kinetics $Y_S^{f/r}(\xi_S)$. When the stress-induced phase transformation kinetics is interpolated by the cosine or exponential function (27) and (28), due to the non-linear nature of cosine and exponential functions, an iterative strategy such as Newton-Raphson scheme (Simo and Hughes 1998) should be utilized to evaluate the value of ξ_S^{n+1}. However, when martensite transformation kinetics is linearly interpolated using Eqs. (27) and (28), it is possible to obtain an exact value for ξ_S^{n+1} through solving linear system of equations. It should be mentioned that for the case of $\varepsilon_{tr} = 0$, which refers to the absence of detwinned martensite, it is not possible to produce martensite phase by applying thermo-mechanical loads. In this case, $\text{sgn}(\varepsilon_{tr})$ can be replaced by $\text{sgn}(\sigma)$ which allows determination of the governing equations for the martensite nucleation process.

2.5 Twinned martensite evolution

After and specifying σ^{n+1} and ξ_S^{n+1} from the previous section, the evolution of the twinned martensitic volume fraction, ξ_T^{n+1}, can be determined by applying the return mapping algorithm on the temperature-induced phase transformation (22b) constrained by the Kuhn-Tucker and consistency conditions (23). The algorithm consists in capturing a trial state for twinned martensite volume fraction $(\xi_T = \xi_T^n)$ and in verifying the admissibility of such a state through the value of the limit function on the trial state, i.e., $F_T(\xi_S^{n+1}, \xi_T^n)$. If the trial state is admissible $(F_T(\xi_S^{n+1}, \xi_T^n) \le 0)$ then twinned martensite does not evolve and the twinned martensite volume fraction ξ_T^n is taken as the updated value (ξ_T^{n+1}). If the trial state is non-admissible $(F_T(\xi_S^{n+1}, \xi_T^n) > 0)$, temperature-induced forward/reverse phase transformation takes place and a new value of ξ_T can be computed by applying consistency conditions (23b) to (22b) and utilizing Eq. (33) as follows

$$\dot{F}_T^f = 0 \Rightarrow \dot{\xi}_T = \frac{\dot{T}}{M_f^0 - M_s^0} \quad with \dot{T} < 0 \tag{38a}$$

$$\dot{F}_T^r = 0 \Rightarrow \dot{\xi}_T = \frac{|\dot{\sigma}| - C\dot{T}}{C(A_f^0 - A_s^0)} \quad with\ \dot{\xi}_T < 0 \tag{38b}$$

It is useful to note that in many engineering applications, pure thermal loading normally occurs in the constant stress. Due to this fact, Eq. (38(b)) can be reduced to

$$\dot{\xi}_T = -\frac{\dot{T}}{(A_f^0 - A_s^0)} \quad with \dot{T} > 0 \tag{39}$$

In this especial case, the rate of twinned martensite is decoupled from system of Eq. (36) and can be directly computed from Eqs. (38a) and (39). Thus, after Eq. (36) is solved and the new value of ξ_S is computed, ξ_T can be updated through the following conditions

$$\dot{\xi}_T = \begin{cases} \dot{T}/(M_f^0 - M_s^0) & F_T^f(T, \xi_T^n) \geq 0 \qquad \dot{T} < 0 \\ -\dot{T}/(A_f^0 - A_s^0) \ if & F_T^r(T, \xi_T^n) \geq 0 \ and \ \dot{T} > 0 \\ -\dot{\xi}_S & \xi_T^n + \xi_S > 1 \end{cases} \tag{40}$$

It is noted that the last of Eq. (40) constrains the total martensite volume fraction to be always less than unity. Furthermore, the relation between the rates of ξ_S and ξ_T allows the model to simulate creation of detwinned martensite at the expense of twinned martensite.

3. Numerical simulations

The present section deals with several uniaxial tension, torsion and bending tests to show the model capability of reproducing main effects of the SMAs such as martensitic phase transformation, shape memory effect, pseudo-elasticity and ferro-elasticity. In particular, Section 3.1 presents some qualitative comparison studies between experimental results and present simulations for uniaxial tension and torsion tests performed in different temperatures. In Section 3.2, the results for bending tests of SMA beams with different thermo-mechanical loading paths are presented and possible comparisons with available experiments are performed. In all the simulations discussed in this section, the SMA material is assumed to be initially in twinned martensite and austenite phases for $T < M_s^0$ and $T \geq M_s^0$, respectively.

3.1 Uniaxial tests

In this section, the model predictions for uniaxial tension and torsion tests are compared with experiments available in the open literature (Šittner *et al.* 2009, Thamburaja and Anand 2002). As the first comparison study, the simulation of uniaxial tension test at various constant temperatures of an *NiTi* wire specimen is performed and compared with experimental data in Fig. 3. Linear, cosine and exponential interpolation functions are used to predict SMA response. For comparison with experiments, datasets from an extensive experimental database available at Roundrobin SMA modeling website (Šittner *et al.* 2009) were adapted. Transformation temperatures, determined by differential scanning calorimetric techniques, were reported as $M_f^0 = 249\,K, M_s^0 = 251\,K, A_s^0 = 256\,K$ and $A_f^0 = 260\,K$ (Šittner *et al.* 2009). In order to achieve the comparison study, the material parameters defined in the present model (i.e., $C, \sigma_s^0, \sigma_f^0, \tilde{\sigma}$ and ε_L) should be identified. Therefore, the material parameters are calibrated to match the uniaxial stress-strain response for simple tension test as illustrated in Fig. 3. The extracted quantities are listed in Table 1 for case *I*. It can be found from Fig. 3 that the linear, cosine and exponential approximations yield to maximum, intermediate and minimum difference with respect to experiment data in the forward phase transformation. However, it is seen that all interpolations

generally result in a similar response in the reverse phase transformation. Fig. 3 also shows that the present model with the aid of the exponential interpolation function reasonably captures changes of the behavior from martensite transformation at low temperatures $(253\,K)$ to pseudo-elastic at higher temperatures $(333\,K)$. Therefore, unless otherwise stated, the exponential form is used to govern the kinetics of stress-induced phase transformation to compute the next results.

To further examine predictive capabilities of the presented model, the results of simple tension and pure torsion experiments with a thin-walled tubular specimen of *NiTi* reported by Thamburaja and Anand (2002) are employed and depicted in Fig. 4. The transformation temperatures were reported as $M_f^0 = 213\,K, M_s^0 = 251.3\,K, A_s^0 = 260.3\,K$ and $A_f^0 = 268.5\,K$ (Thamburaja and Anand 2002). The specimens were tested at room temperature $(T = 298\,K = A_f^0 + 29.5\,K)$ under simple tension and pure torsion loadings. Similar to the previous example, the material parameters are identified using the experimental data as depicted in Fig. 4 which are listed in Table 1 for the case *II*. Fig. 4 shows the comparison between predictions of the proposed model and experimental data for tension and torsion tests. This figure reveals that the present model is able to accurately simulate the main characteristics of both uniaxial tension and torsion tests. A good qualitative agreement is obtained with the same parameters for both tension and torsion responses. It should be noted that the experiments exhibit some residual strains after complete unloading of the specimen. This is most probably due to plastic deformation of the austenite and some stabilized martensite (Saleeb *et al.* 2013), effects of which are not taken into account in the present constitutive model and consequently are not predicted by the model.

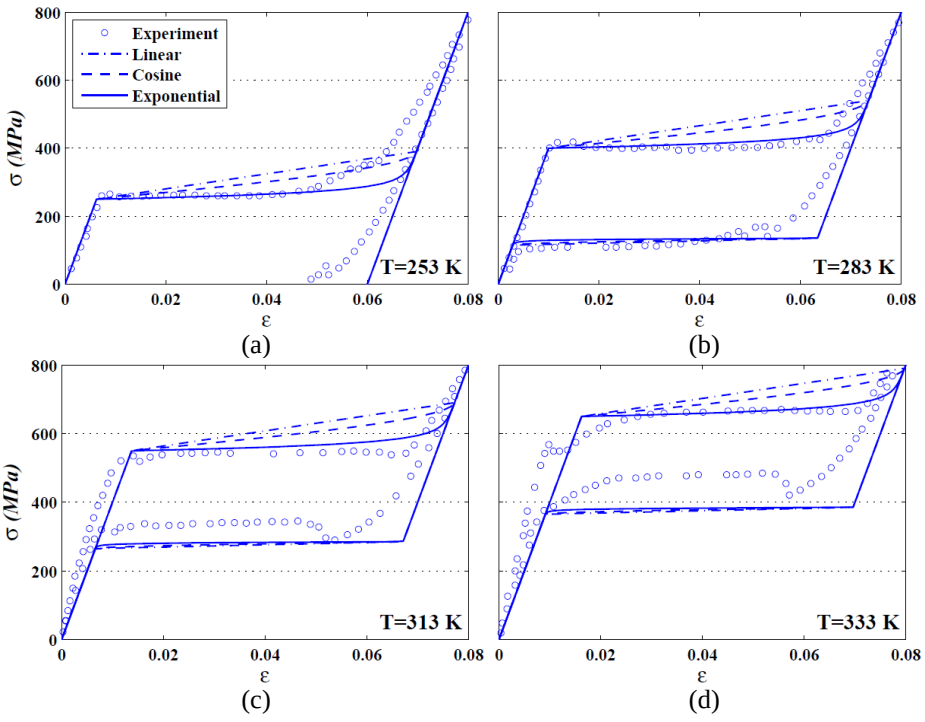

Fig. 3 Model predictions compared to the experimental data (Šittner *et al.* 2009) for simple tension tests in different temperatures

Table 1 Material parameters used in the numerical tests

	Material parameters							
Case	E [a]	ρ [b]	ν	$\tilde{\sigma}$ [a]	σ_s^0 [a]	σ_f^0 [a]	C [c]	ε_L
I	40000	6500	0.33	1	240	380	5	0.06
II	50000	6500	0.33	600	157.53	501.04	3	0.1308
III	60000	8000	0.33	80	72	452.5	8.5	0.075

[a]Unit: MPa

[b]Unit: kg/m^3

[c]Unit: MPa/K

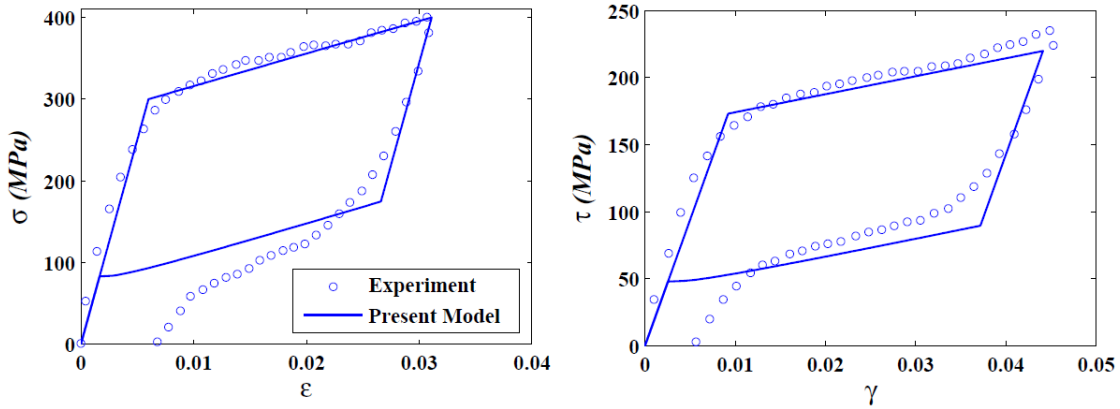

(a) (b)

Fig. 4 Comparison between model predictions and experimental data (Thamburaja and Anand 2002): (a) simple tension test and (b) pure torsion test

Moreover, experimental results reveal that the martensitic phase transformation in SMAs is associated with generation or absorption of latent heat in forward and reverse transformations. The self-heating and self-cooling due to latent heat of phase transformation and also heat transfer due to external temperatures affect the position and shape of the hysteresis cycle (Mirzaeifar *et al*. 2011, Torra *et al*. 2013). Since the main focus of the presented model is on the primary effects of SMAs, the secondary effects such as permanent inelasticity and self-heating/cooling and heat transfer of the SMA materials could be considered to improve the present model. The reader is referred to (Mirzaeifar *et al*. 2011, Saleeb *et al*. 2013, Torra *et al*. 2013) and references therein for examples of advancements in modeling of these mechanisms.

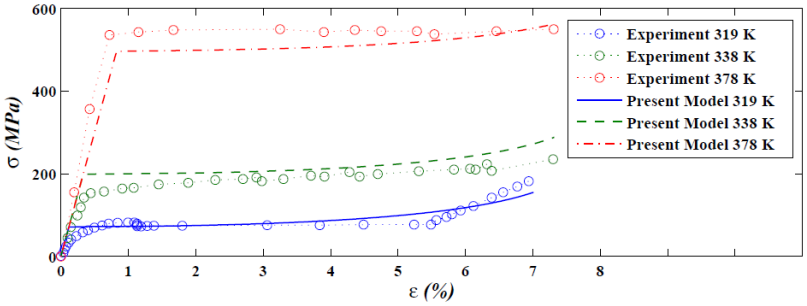

Fig. 5 Model prediction compared to the experimental data (Flor *et al.* 2006) for simple tension tests in different temperatures

3.2 Bending tests

In this section, results obtained from the present model for bending tests of *NiTi* cantilever beams under different thermo-mechanical loading paths are demonstrated and possible comparisons with experiments reported in Flor *et al.* (2006) are presented. Four characteristic transformation temperatures were reported as $M_f^0 = 297\,K, M_s^0 = 323\,K, A_s^0 = 348\,K$ and $A_f^0 = 355\,K$ (Flor *et al.* 2006). The material parameters are identified by means of experimental results reported by Flor *et al.* (2006) for uniaxial tensile tests at three different temperatures 319, 338 and 378 *K*, as shown in Fig. 5. This figure also shows the model predictions for these tests. The material properties are tabulated in Table 1 for case *III*. In order to simulate bending tests of thin *NiTi* beams, a finite element solution is developed by computer programming with *MATLAB*®. Details of the finite element formulation are given in Appendix. The SMA beam with 60 mm length has a circular cross section with diameter of 1 mm. It has clamped boundary conditions at one end while the other end is free.

For the first structural simulation, the *NiTi* cantilever beam experiences an upward point load with the maximum magnitude of *F* at the free end. Figs. 6(a) and 6(b) illustrate the simulated load-tip deflection response of the cantilever beam at $T = 323$ and $378\,K$, respectively. Experimental data reported by Flor *et al.* (2006) are also included in Fig. 6. A good qualitative correlation between the experimental data and prediction of the proposed model can be observed. It can also be seen that the critical transformation stresses increase with the temperature, as expected experimentally and theoretically (see Eq. (35)). The counterparts of Figs. 6(a) and 6(b) for the *NiTi* cantilever beam under symmetrical bending cycles are depicted in Figs. 7(a) and 7(b), respectively. The beam free end is first loaded upward and then unloaded. Next, the structure undergoes a loading-unloading step in the downward direction. Fig. 7 shows that the model is able to reproduce the characteristic hysteresis loops of SMAs in the tension-compression path at both low and high temperatures. Furthermore, the simulation results presented in Figs. 7(a) and 7(b) demonstrate the ability of the model to reproduce ferro-elasticity and pseudo-elasticity at low and high temperatures. Finally, it should be mentioned that, 1-D SMA components in many structural engineering applications experience tensile and compressive cycles, see for instance Daghia *et al.* (2010). Therefore, the modeling of ferro-elasticity effect of low-temperature SMAs under tension-compression loadings is essential since it is the single mechanism of deformation.

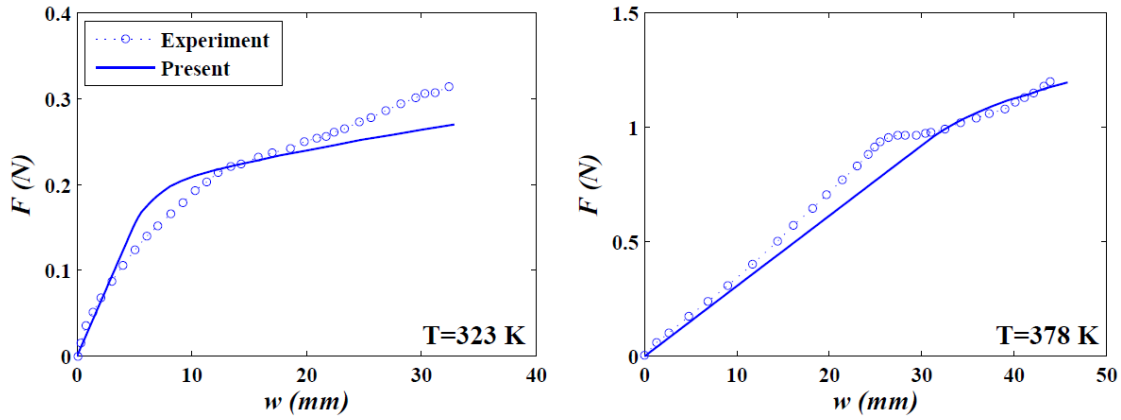

Fig. 6 Model prediction compared to the experimental data (Flor *et al*. 2006) for bending tests at (a) 323 and (b) 378 *K*

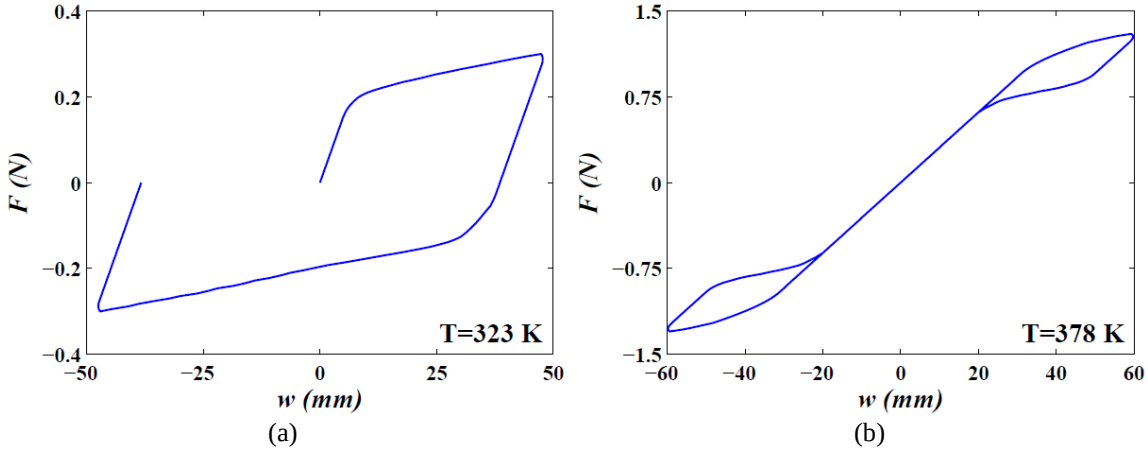

Fig. 7 Model prediction for the *NiTi* cantilever beam under symmetrical bending cycles at (a) 323 and (b) 378 *K*

In order to test the model reproduction of the shape memory effect, bending response of the *NiTi* cantilever beam under thermo-mechanical loadings is studied. Fig. 8 shows the result of this simulation in the $F-T-w$ space and thermo-mechanical loadings as *A*-*B*-*C*-*B* path. At low temperature of $323\,K$, the beam free end is loaded up to the maximum force of $0.3\,N$. As it can be seen in Fig. 8, the material initially in austenite phase transforms to detwinned martensite affecting slope of $F-w$. In the next stage, maintaining the tip point load, the *NiTi* beam is heated up to $358\,K\,(=A_f^0+3K)$. By heating, the inelastic strain disappears due to temperature driven reverse phase transformation leading to deflection recovery. Note that an elastic deformation remains in the beam due to the presence of tip point load. Finally, cooling the SMA

beam, while the load is still applied, results in the direct formation of detwinned martensite producing inelastic strain and deformation. It is interesting to note that the cooling process returns tip deflection to original point prior to heating.

4. Conclusions

In this research work, a simple and efficient 1-D constitutive model of shape memory alloys was proposed with capability of the ferro-elastic simulation. The SMA model was established within the framework of thermodynamics of irreversible processes in the realm of small strain regime. The model nominated the volume fractions of twined and detwinned martensite as internal variables. The Helmholtz free energy function was constructed and thermodynamic driving forces of internal variables were obtained from the dissipative inequality. Linear, cosine and exponential functions were introduced in a unified framework to interpolate the martensite transformation kinetics and the analytical description of the constitutive equations was presented. Introducing a simple procedure, the material and kinetic parameters defined in the present model were expressed in terms of four characteristic temperatures and five quantities that calibrated to match the uniaxial stress-strain response for simple tension-compression and/or pure torsion+/ experimental tests. A qualitative comparison study was first carried out between the results of the present simulations using different interpolation functions and experimental data available in the open literature for simple tension and pure torsion tests. The simulations revealed that the use of exponential interpolation function for the martensite transformation kinetics leads to an accurate response in comparison with experiments. Then, a finite element formulation was established to simulate experimental bending tests of thin SMA cantilever beams. Finally, the developed SMA model and finite element solution were implemented to study bending response of SMA cantilever beams under various thermo-mechanical loadings accompanied with martensitic phase transformation, shape memory effect, pseudo-elasticity and in particular ferro-elasticity. Due to simplicity and accuracy of the presented model, it is expected that the model to be used to predict one-dimensional behavior of SMA components in various structural engineering applications particularly when the ferro-elasticity is obvious.

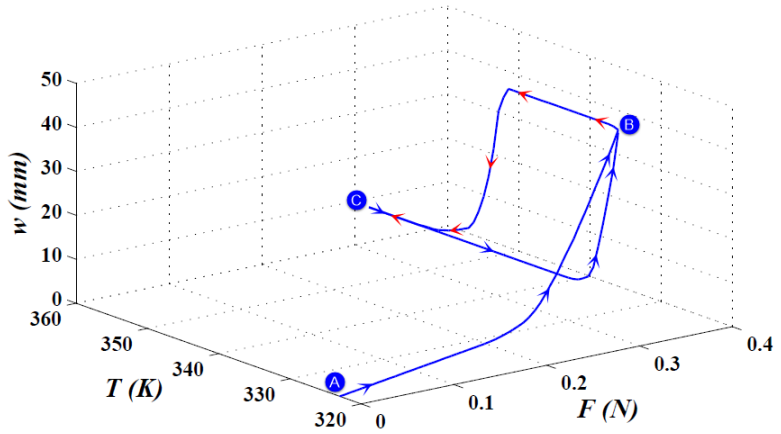

Fig. 8 Model prediction for the *NiTi* cantilever beam under thermo-mechanical loadings in *F-T-w* space

Acknowledgments

The work described in this paper was partially supported by grants from the Research Grants Council of the Hong Kong Special Administrative Region, China (Project Nos. CUHK414712 and T23-407/13-N).

References

Brinson, L.C. (1993), "One-dimensional constitutive behavior of shape memory alloys: Thermomechanical derivation with non-constant material functions and redefined martensite internal variable", *J. Intel. Mat. Syst. Struct.*, **4**(2), 229-242.

Boyd, J.G. and Lagoudas, D.C. (1996), "A thermodynamical constitutive model for shape memory materials Part I: The monolithic shape memory alloy", *Int. J. Plast.*, **12**, 805-842.

Bekker, A. and Brinson, L.C. (1998), "Phase diagram based description of the hysteresis behavior of shape memory alloys", *Acta Mater*., **46**, 3649-3665.

BenMekki, O. and Auricchio, F. (2011), "Performance evaluation of shape-memory-alloy superelastic behavior to control a stay cable in cable-stayed bridges", *Int. J. Nonlinear Mech.*, **46**, 470-477.

Bodaghi, M., Damanpack, A.R., Aghdam, M.M. and Shakeri, M. (2013), "A phenomenological SMA model for combined axial-torsional proportional/non-proportional loading conditions", *Mater. Sci. Eng. A.*, **587**, 12-26.

Casciati, S. and Hamdaoui, K. (2008), "Experimental and numerical studies toward the implementation of shape memory alloy ties in masonry structures", *Smart Struct. Syst.*, **4**(2), 153-169.

Chung, J.H., Heo, J.S. and Lee, J.J. (2007), "Implementation strategy for the dual transformation region in the Brinson SMA constitutive model", *Smart Mater. Struct.*, **16**, 1-5.

Carreras, G., Casciati, F., Casciati, S., Isalgue, A., Marzi, A. and Torra, V. (2011), "Fatigue laboratory tests toward the design of SMA portico-braces", *Smart Struct. Syst.*, **7**(1), 41-57.

Daghia, F., Inman, D.J., Ubertini, F. and Viola, E. (2010), "Active shape change of an SMA hybrid composite plate", *Smart Struct. Syst.*, **6**(2), 91-100.

Flor, S.D., Urbina, C. and Ferrando, F. (2006), "Constitutive model of shape memory alloys: theoretical formulation and experimental validation", *Mater Sci. Eng. A.*, **427**, 112-122.

Liang, C. and Rogers, C.A. (1990) "One-dimensional thermomechanical constitutive relations for shape memory materials", *J. Intel. Mat. Syst. Str.*, **1**(2), 207-234.

Lagoudas, D.C., Bo, Z. and Qidwai, M.A. (1996) "A unified thermodynamic constitutive model for SMA and finite element analysis of active metal matrix composites", *Mech. Compos. Mater. Struct.*, **3**, 153-179.

Lexcellent, C., Boubakar, M.L., Bouvet, C. and Calloch, S. (2006), "About modelling the shape memory alloy behaviour based on the phase transformation surface identification under proportional loading and anisothermal conditions*", Int. J. Solids Struct.*, **43**(3-4), 613-626.

Lagoudas, D.C. (2008), *Shape Memory Alloys: modeling and engineering applications*, Springer, New York, USA.

Mirzaeifar, R.,·DesRoches, R. and Yavari, A. (2011), "Analysis of the rate-dependent coupled thermo-mechanical response of shape memory alloy bars and wires in tension", *Continuum Mech. Therm.*, **23**, 363-385.

Patoor, E., Lagoudas, D.C., Entchev, P.B., Brinson, L.C. and Gao, X. (2006), "Shape memory alloys, Part I: General properties and modeling of single crystals", *Mech. Mater.*, **38**, 391-429.

Panico, M. and Brinson, L.C. (2007), "A three-dimensional phenomenological model for martensite reorientation in shape memory alloys", *J. Mech. Phys. Solids.*, **55**, 2491-2511.

Roh, J.H., Oh, I.K., Yang, S.M., Han, J.H. and Lee, I. (2004), "Thermal post-buckling analysis of shape memory alloy hybrid composite shell panels", *Smart Mater. Struct.*, **13**, 1337-1344.

Simo, J.C. and Hughes, T.J.R. (1998), *Computational Inelasticity*, Springer, New York, USA.

Šittner, P., Pilch, J. and Heller, L. (2009) <http://ofm.fzu.cz/ofm/index.php/en/roundrobin>.
Seelecke, S. and Muller, I. (2004), "Shape memory alloy actuators in smart structures: Modeling and simulation", *Appl. Mech. Rev.*, **57**, 23-46.
Shahria Alam, M., Nehdi, M. and Youssef, M.A. (2009), "Seismic performance of concrete frame structures reinforced with superelastic shape memory alloys", *Smart Struct. Syst.*, **5**(5), 565-585.
Saleeb, A.F., Kumar, A., Padula, S.A. and Dhakal, B. (2013), "The cyclic and evolutionary response to approach the attraction loops under stress controlled isothermal conditions for a multi-mechanism based multi-axial SMA model", *Mech. Mater.*, **63**, 21-47.
Sedlák, P., Frost, M., Benešová, B., Ben Zineb, T. and Šittner, P. (2012), "Thermomechanical model for NiTi-based shape memory alloys including R-phase and material anisotropy under multi-axial loadings", *Int. J. Plast.*, **39**, 132-151.
Tanaka, K. (1986), "A thermomechanical sketch of shape memory effect: One-dimensional tensile behavior", *Res. Mechanica.*, **18**, 251-263.
Thamburaja, P. and Anand, L. (2002), "Superelastic behavior in tension–torsion of an initially-textured Ti–Ni shape-memory alloy", *Int. J. Plast.*, **18**(11), 1607-1617.
Torra, V., Auguet, C., Isalgue, A., Carreras, G., Terriault, P. and Lovey, F.C. (2013), "Built in dampers for stayed cables in bridges via SMA. The SMARTeR-ESF project: A mesoscopic and macroscopic experimental analysis with numerical simulations", *Eng. Struct.*, **49**, 43-57.
Youssef, M.A. and Elfeki, M.A. (2012), "Seismic performance of concrete frames reinforced with superelastic shape memory alloys", *Smart Struct. Syst.*, **9**(4), 313-333.
Zhang, Y. and Zhao, Y.P. (2007), "A study of composite beam with shape memory alloy arbitrarily embedded under thermal and mechanical loadings", *Mater. Design*, **28**(4), 1096-1115.

FC

Appendix: Modeling of SMA beams under bending tests

A finite element formulation is developed here to simulate bending response of thin SMA beams under various thermo-mechanical lodgings. Cartesian coordinate system (*x*, *z*) is located on the mid-plane of beam where *x* is the beam axial direction, whereas *z* denotes the upward transverse direction. The displacement field of the SMA beam is assumed based on the Euler-Bernoulli beam theory as

$$\begin{aligned} \overline{u}(x,\, z) &= u(x) - z\, w'(x) \\ \overline{w}(x, z) &= w(x) \end{aligned} \tag{A.1}$$

where u and w are displacements of the mid-surface of the beam along the x and z directions, respectively. Also, the prime on a variable indicates its derivative with respect to x.

Using Eq. (A.1), the axial strain can be expressed as

$$\varepsilon = u' - z\, w'' \tag{A.2}$$

In order to derive the governing equations of equilibrium for the SMA beam, the principle of minimum total potential energy is utilized as

$$\delta U - \delta W = 0 \tag{A.3}$$

where δU and δW are the virtual strain energy and applied external work, respectively. Using Eq. (36) for stress, δU can be written as

$$\delta U = \int_V \delta\varepsilon^T \sigma\, dV = \int_V \delta\varepsilon^T E\varepsilon\, dV - \int_V \delta\varepsilon^T E(\varepsilon_{tr} - \varepsilon_{tr0})\, dV \tag{A.4}$$

where V denotes the SMA element volume and ε_{tr0} is the initial martensitic residual strain along the *x* direction (pre-strain) in the SMA element.

The virtual external work done by axial (P_1 , P_2) and transverse shear (V_1,V_2) forces and bending moment (M_1,M_2) on the first and end nodes of the element can be written as

$$\delta W = P_1\, \delta u_1 + P_2\, \delta u_2 + V_1 \delta w_1 + V_2 \delta w_2 + M_1 \delta\theta_1 + M_2 \delta\theta_2 \tag{A.5}$$

where u_1 , w_1 and u_2 , w_2 are axial and transverse displacements of the first and the end nodes of the element whereas parameter θ refers to $-w'$.

The axial displacement $u(x)$ and transverse deflection $w(x)$ are approximated as

$$\begin{aligned} & u(x) = \mathbf{N}\mathbf{u} \;\; ; \;\; w(x) = \overline{\mathbf{N}}\mathbf{u} \\ & \mathbf{N} = \begin{Bmatrix} N_1 & 0 & 0 & N_2 & 0 & 0 \end{Bmatrix} \\ & \overline{\mathbf{N}} = \begin{Bmatrix} 0 & \overline{N}_1 & \overline{N}_2 & 0 & \overline{N}_3 & \overline{N}_4 \end{Bmatrix} \\ & \mathbf{u} = \begin{Bmatrix} u_1 & w_1 & \theta_1 & u_2 & w_2 & \theta_2 \end{Bmatrix}^T \end{aligned} \tag{A.6}$$

where $\mathbf{u}$ is the nodal variables vector while $N_i\,(i=1,2)$ and $\overline{N}_i\,(i=1..4)$ are the linear Lagrange and Hermite cubic interpolation functions defined as:

$$
\begin{aligned}
N_1 &= 1 - x/l \\
N_2 &= x/l \\
\overline{N}_1 &= 1 - 3(x/l)^2 + 2(x/l)^3 \\
\overline{N}_2 &= x(1 - x/l)^2 \\
\overline{N}_3 &= 3(x/l)^2 - 2(x/l)^3 \\
\overline{N}_4 &= x((x/l)^2 - x/l)
\end{aligned}
\tag{A.7}
$$

The strain field of the beam element can also be expressed in terms of mechanical nodal variables as

$$
\begin{aligned}
\varepsilon &= \mathbf{B}\mathbf{u} \\
\mathbf{B} &= \mathbf{N}' - z\overline{\mathbf{N}}''
\end{aligned}
\tag{A.8}
$$

By substituting the strain field (A.8) into the strain energy (A.4) and subsequent results into the principle of minimum total potential energy (A.3), the governing equations of equilibrium can be derived as

$$
\mathbf{K}\mathbf{u} = \mathbf{F}_{tr} + \mathbf{F} \tag{A.9}
$$

where

$$
\begin{aligned}
\mathbf{K} &= \int_V E\,\mathbf{B}^T\mathbf{B}dV \\
\mathbf{F}_{tr} &= \int_V E\,\mathbf{B}^T(\varepsilon_{tr} - \varepsilon_{tr0})dV \\
\mathbf{F} &= \begin{Bmatrix} P_1 & V_1 & M_1 & P_2 & V_2 & M_2 \end{Bmatrix}^T
\end{aligned}
\tag{A.10}
$$

Note that the transformation strain ε_{tr} is variable through the SMA element domain in both *x* and *z* directions. However, it is assumed that ε_{tr} to be constant along the SMA element length while the Gauss-Legendre numerical integration rule is utilized to evaluate the through-the-thickness integral consists of ε_{tr}.

Finally, Eq. (A.9) is utilized to generate global finite element vectors and matrices by assembly and application of boundary conditions which leads to

$$
\overline{\mathbf{K}}\overline{\mathbf{u}} = \overline{\mathbf{F}}_{tr} + \overline{\mathbf{F}} \tag{A.11}
$$

Eq. (A.11) is an algebraic equation in terms of mechanical nodal variables and nodal transformation strain which are distributed through the thickness of each SMA element. Theses inelastic nodal variables should be computed using SMA constitutive equations described in Section 2.4 in framework of an elastic-predictor inelastic-corrector return map procedure, see Simo and Hughes (1998) for more details.

The simulation of bending tests of SMA beams presented in Section 3.2 is performed by assuming 20 elements in the axial direction and implementing 7 through-the-thickness Gauss points per element to obtain the converged results up to two significant digits. Furthermore, it is assumed that the SMA temperature is uniformly raised by ignoring self-heating/cooling due to latent heat of phase transformation and also heat transfer due to external temperatures.